Copyright 2001, Society of Photo-Optical Instrumentation Engineers
This material was presented at SPIE's 26th Annual International Symposium on Microlithography as presentation number 4346-72 and is made available as an electronic reprint with permission of SPIE. One print or electronic copy may be made for personal use only. Systematic or multiple reproduction, distribution to multiple locations via electronic or other means, duplication of any material in this paper for a fee or for commercial purposes, or modification of the content of the paper are prohibited.

Multiple Pitch Transmission and Phase Analysis of Six Types of Strong Phase-Shifting Masks

David J. Gerold[a], John S. Petersen[a], and Marc. D. Levenson[b]

[a]Petersen Advanced Lithography, Inc., 8834 N. Capital of Texas Highway, #304, Austin, TX 78759
[b]M.D. Levenson Consulting, 19868 Bonnie Ridge Way, Saratoga, CA 95070

ABSTRACT

Our previous work showed that for 100nm lines, the Sidewall Chrome Alternating Aperture (SCAA) mask structure could overcome the problem of transmission and phase imbalance among multiple pitch structures[1]. In that work, we explained the SCAA mask concept, showed a brief electromagnetic field (EMF) simulated comparison to two subtractive etch techniques and proposed a fabrication paradigm that could make SCAA a reality. What we did not show, however, was the detail of our EMF simulation work for any of these masks.

Our current work provides this missing item and explores across pitch performance at 248nm wavelength for several masks meant to optimize alternating phase-shift (altPSM) mask phase and transmission: SCAA, asymmetric lateral biased, additive, undercut, dual trench (with and without undercut), mask-phase-only, and uncompensated. First, we discuss why vector electromagnetic field (EMF) simulation is necessary. Then we describe a typical optimization approach. There we describe how two simulators, ProMAX (FINLE Technologies, Inc.) and TEMPESTpr (Panoramic Technologies), were set up to reduce grid snapping and other simulation pitfalls, as well as EMF output analysis and topography optimization techniques using one mask type as an example. The optimization approach was to find the best topography for the 100:200nm line:space mask of each type according to the phase and transmission errors extracted from the EMF simulated diffraction orders. Because phase and transmission errors in an alternating PSM are both coupled to the existence of a non-zero central diffraction order[2], we screened mask topographies according to the zero diffraction order power, relative to power in the first orders. Monitoring the central diffraction order did prove be a useful technique for optimizing topographies because it is a single attribute that correlates to both phase and transmission errors, which are coupled and thus difficult to optimize concurrently. The same topography adjustments from the 300nm pitch optimization were then applied through pitch with fixed 100nm line.

Next we summarize the EMF results for each mask compensation technique. Mask types were ranked according to best sum of central diffraction order power through pitch, effectively ranking phase and transmission performance across pitch by mask type. The highest ranking masks were SCAA (with 15nm ARC on chrome and no topography adjustments from ideal) and the asymmetric biased mask (with no ARC but with 40nm increase in each side of shifter space width at mask scale). The lowest performing masks were dual-trench (mainly because of phase errors) and the unadjusted mask (mainly due to transmission errors).

Finally we move from EMF to lithographic simulation of the best two masks according to EMF simulation. For SCAA and asymmetric bias we examine the NILS and MEEF (with line size 90nm, 100nm, and 110nm) for 300nm pitch. Responses for the process window analysis include resist linewidth, resist retention, sidewall angle and feature placement. The analysis showed that SCAA and optimized asymmetric bias had identical NILS through focus, but that image CD was less sensitive to focus on a SCAA mask than on an asymmetric biased mask. The MEEF results were 0.9 for both masks, while SCAA had better depth of focus than the asymmetric biased mask for single line sizes.

While the asymmetric biased mask is simpler to build with existing mask production processes, it requires EMF simulation to determine optimum topography (as do all the other compensation techniques in this study). SCAA requires a non-standard chrome deposition, but performed well according to lithographic simulations without any EMF simulation and topography adjustment. Both SCAA and asymmetric biased masks, it should be noted, did not require any undercut. Future work aimed at the most promising altPSM mask types is needed to further quantify sensitivity to expected fabrication variations and to gain experience with physical wafer prints.

Keywords: alternating PSM, phase shift mask, SCAA, dual trench, EMF simulation, ProMAX, PROLITH, TEMPEST

1. INTRODUCTION

Our previous work showed that for 100 nm lines, a sidewall chrome alternating aperture (SCAA) mask could overcome the problem of transmission and phase imbalance among multiple pitch structures. In that work, we explained the SCAA mask structure, showed an EMF comparison to two subtractive etch techniques, and proposed a fabrication infrastructure paradigm that could make SCAA a reality. Current work extends EMF comparison to other topographies and explores the lithographic potential of the most promising candidates.

There are many ways to make an alternating phase shift mask. Generally the fabrication techniques fall under two categories: the subtractive etch process or the additive process. The additive process is oldest, first produced by one of the authors[3] and independently patented but not fabricated by Shibuya[4]. The other techniques are all subtractive. The first was simply a subtractive etch to create the phase difference between the alternating apertures. This type of alternating phase shift mask showed a problem with the intensity between the alternating phase apertures where the phase cut aperture was the darker of the two. Through the years, research groups have tried to solve this problem; their work has resulted in several papers. Ferguson et. al. examined asymmetric bias, quartz undercut of the chrome line, and dual trench techniques to fix the transmission problem, and observed that there was an apparent phase error induced as the pitch changed[5]. However, their work was restricted to features with one-to-one duty cycles. Terasawa et al and Kanai et al showed that a dual trench technique could correct the phase and transmission problem for a given pitch. They too examined features with one -to-one duty cycles[6,7]. The dual trench showed promise because it could optimize phase and transmission without undercut— significant because an undercut can compromise mechanical strength of the chrome on quartz. Petersen and other authors also studied the dual trench technique in two different papers[8, 9]. Again, the studies were limited in that they dealt with single pitch and line duty. In 1992 Levenson first proposed the SCAA mask[10]. SCAA mitigates the phase and transmission problems of the trench techniques and, because chrome is everywhere supported by quartz , offers mechanical strength. SCAA's shortcoming is that the non-critical phase level is written first and the critical binary level is written last. This scheme raises manufacturing costs if plates have to be scrapped for any reason. The "Phase Phirst" approach, where blanks are produced ahead of time with a pre-patterned phase layer underneath chrome and resist films, addresses fabrication and cost issues. To be successful, the approach requires writing a large number of standardized blanks. Still, because of SCAA's positive attributes, these issues should be addressed.

This paper explores across pitch performance of several mask types (Figure 1): SCAA, asymmetric lateral biased, additive, undercut, dual trench (with and without undercut), mask-phase-only, and uncompensated alternating phase-shift masks. Mask-phase-only implies that only the shifter trench is adjusted. Uncompensated (or "geometric") means no correction is applied beyond geometric phase depth expected from scalar theory. First, we discuss why vector electromagnetic field (EMF) simulation is necessary and describe a typical optimization approach. There we describe how two simulators, ProMAX (FINLE Technologies, Inc.) and TEMPESTpr (Panoramic Technologies), were set up to reduce grid snapping and other simulation pitfalls, as well as EMF output analysis and topogr aphy optimization techniques using one mask type as an example. The optimization approach was to find the best topography for the 100:200nm line:space mask of each type according to the phase and transmission errors extracted from the EMF simulated diffraction orders. The same topography adjustments from the 300nm pitch optimization were then applied through pitch with fixed 100nm line.

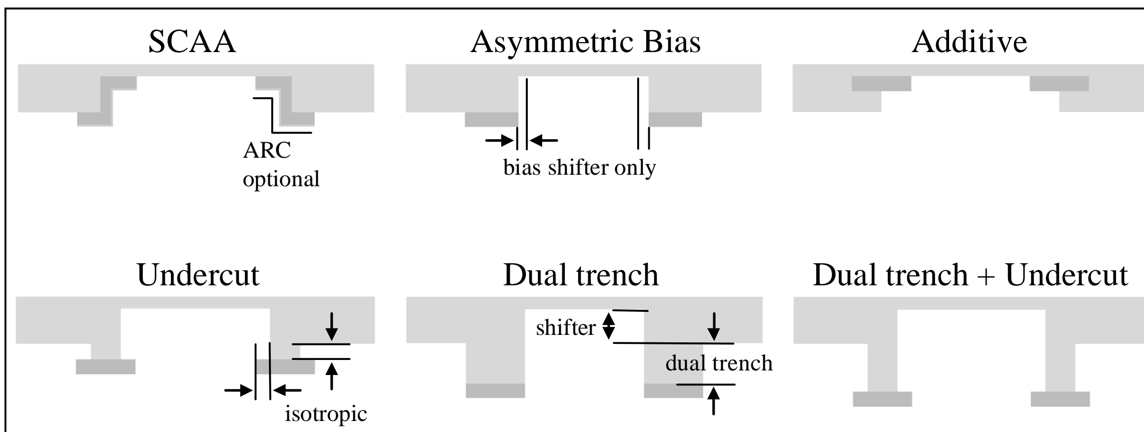

Figure 1: Types of masks for adjusting phase and transmission

Next we summarize the EMF results for each mask compensation technique, and finally, move to lithographic simulation of the best two masks according to EMF simulation (SCAA and asymmetric bias masks), examining NILS and MEEF.

2. ELECTROMAGNETIC SIMULATION AND OPTIMIZATION

The Motivation for Using Electromagnetic Simulators of Mask Topography

The shifter etch depth in an alternating phase shift mask is typically calculated according to

$$\Delta\varphi = 2\pi d(n-1)/\lambda \quad (1)$$

where:
$\Delta\varphi$ is the phase shift
d is the difference in depth between shifted and unshifted spaces,
n is the index of refraction, and
λ the wavelength.
It is well known that a phase shift mask with perfectly accurate etch depth according to Equation 1 shows non-ideal phase shift and unequal transmission between the shifted and unshifted spaces. Figure 2 shows transmission imbalance, which is also a function of focus.
Scalar lithographic simulators do not currently predict this observed behavior and so electromagnetic field (EMF) vector simulations of Maxwell's equations are required to more closely predict actual mask fields. Our work used the EMF simulators ProMAX (a 2-D simulator) from FINLE Technologies, Inc. and TEMPESTpr (a 3-D simulator), from Panoramic Technologies. The field intensity and phase output of the EMF simulator at a plane just below the mask was exported as a “grayscale” mask for input to PROLITH.

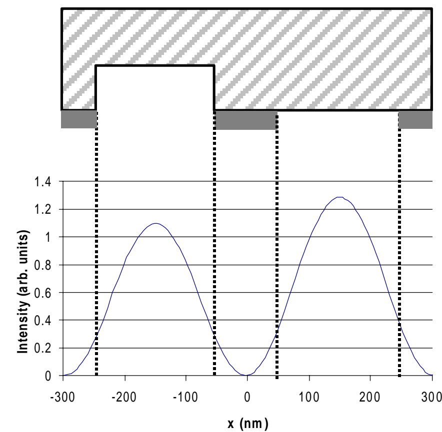

Figure 2: Unequal transmission not predicted by scalar simulators

Alternating PSM Topography Design Approach

Our approach in this work was to optimize the 300nm pitch (100nm line, 200nm space) mask of each type first and then apply the same adjustment values across pitch to study across pitch performance. Each mask had a fixed line size of 100nm and pitch varying from 200nm to 1100nm. Figure 3 outlines this sequence.

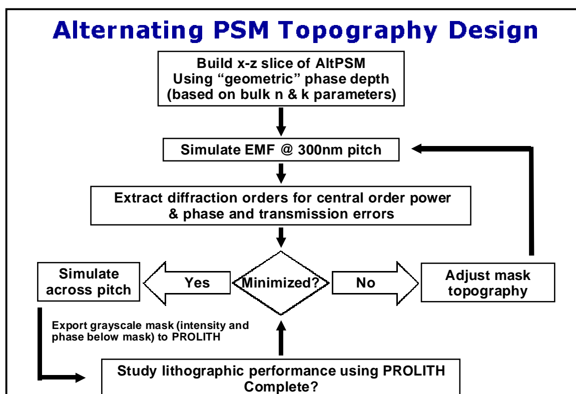

Figure 3: Mask topography design approach

Optimizing a given topography required iterating between the mask’s unique attribute (e.g. undercut or asymmetric bias) and the more generic shifter etch depth. In general one could not separate the phase and transmission effects of a given adjustment because they are coupled. A more efficient approach was found to be monitoring the central diffraction order (normalized to the sum of first order powers), because in an ideal 180 degree shifted PSM the central diffraction order will have zero amplitude[11]. Minimizing the central diffraction order will tend to minimize combined phase and transmission errors concurrently. In this paper, phase error will be defined as (effective phase - 180 degrees) and transmission error as (t1-t2), where t1 is transmission through the shifted space and t2 is transmission through the unshifted space. Mask types to be explored here were outlined in Figure 1.

EMF Simulator Setup

Several parameters common to EMF mask simulators require characterization and attention to produce the best results. First, “gridding” issues must be addressed. Both ProMAX and TEMPESTpr are finite difference time domain (FDTD) simulators, which implies that mask geometries are divided into cells on a fixed grid in each direction. Both ProMAX and TEMPESTpr allow one to set grid size independently in each direction. This ability is crucial to avoid unnecessarily large numbers of cells causing long simulation time and large memory usage.

The choice of grid is in general a tradeoff between accuracy and resources, including simulation time. We follow a rule of thumb in EMF and lithographic simulations of setting 5-10 points per smallest feature to be resolved, but this can be adjusted as each simulator is characterized for behavior as a function of decreasing grid size. One test related to accuracy is the "vacuum test" to vary vertical step size while simulating light propagating through a vacuum (with index n,k equal to 1,0) and with the same n and k at each boundary. In theory the result should be a uniform intensity (1.0 in our case) throughout the material. In practice, both simulators produce standing waves with varying intensity in the vertical direction, which may be related to matching boundary conditions at simulation boundaries. The amplitude of the standing waves, or the "vacuum test range" is one factor limiting simulator accuracy and is a useful tool for benchmarking accuracy. Figures 4 show that ProMAX standing wave peak-to-peak range decreases as step size decreases to at least 0.5nm at λ=248nm (or 496 steps per wavelength). TEMPESTpr has an optimum step size below which standing wave peak-to-peak range increases. This optimum was at 2nm vertical step size, or 124 steps per wavelength. In addition, TEMPESTpr had better standing wave range at large step sizes, but ProMAX was able to use smaller step sizes. These results were obtained with ProMAX version dated Jan. 21, 2001 using simulation "duration" of 3, and TEMPESTpr version 2.03. The horizontal grid size was fixed at 5nm. It is possible that the ratio of horizontal to vertical step size affects standing wave results [12], and such questions are the subject of future work. Because each simulator continues to develop, the users must perform similar qualifications for their own simulator and specific applications.

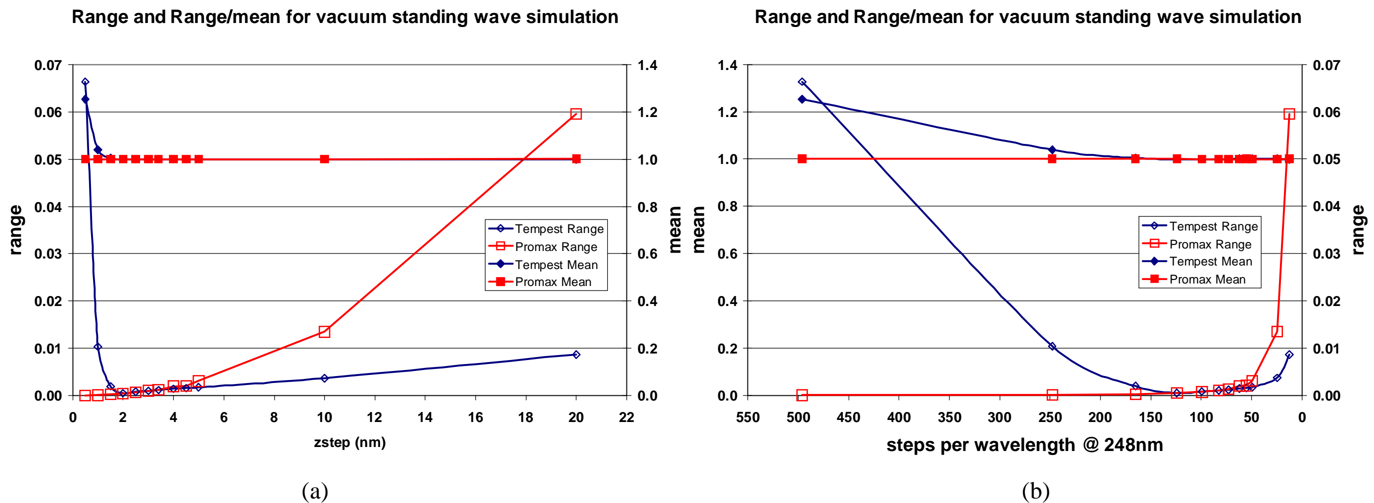

(a) (b)

Figure 4: Mean and range of intensity for benchmarking simulation of vacuum region. Mean intensity would ideally be 1.0 and peak-to-peak standing wave range would be zero. (a) Plotted against vertical step size ("z-step") (b) Plotted against steps per 248 nm wavelength

In addition, grid size must be small enough to resolve the features of interest. For simulating phase shift masks, we rounded all mask coordinates to the intended simulation step sizes and calculated the resulting trench depth, as well as resulting phase shift vs. desired phase shift. In this way we avoided simulator grid snap issues, and monitored how much shift error we were introducing simply by quantizing the trench on a grid. For example, 180 degree phase shift ideally requires a 242.9nm shifter depth, according to equation 1 for λ=248nm wavelength and a quartz reticle blank. A 1.0nm shifter depth error at these conditions would cause a 0.70 degree phase shift design error. Simulator step sizes in our work were chosen to minimize such designed-in phase shift errors, keeping phase error below 0.2 degrees in 96% of 343 simulations. 99% of the simulations used z-step (vertical step) sizes between 1.0nm and 3.4nm. Note that a large step size may cause zero shifter depth error (and vice-versa), but must be played against simulator accuracy vs. step size discussed earlier.

We chose to compare mask types with publicly available[13] bulk chrome n and k parameters 0.85 and 2.01, and assumed 100nm thick chrome. Commercial photomasks have a more complex absorber structure of chrome and anti-reflection materials with composition a function of depth in absorber, so a lithographer must obtain the best estimate of actual absorber parameters for the photomasks of interest.

Finally, the thickness of bulk glass above any topography in the mask cross-sections was constant $\lambda/2$ (82.1nm at λ=248nm).

In short, an EMF simulator must be characterized and set-up for the particular application in question, with particular attention to gridding effects.

EMF Simulation Analysis

In our work we analyzed the mask diffraction pattern directly to quantify and screen EMF results before advancing to lithographic simulation. The techniques involved monitoring the central diffraction order, computing effective phase shift, and computing transmission difference between shifted and unshifted spaces.

Because phase and transmission errors in an alternating PSM are both coupled to the existence of a non-zero central diffraction order[14], we screened mask topographies according to the central order power ratio CPR

$$CPR = A_0^2 / 2*A_1^2 \qquad (2)$$

where A_0 is the central diffraction order amplitude and A_1 is the first diffraction order amplitude. To extract effective phase shift and transmission from ProMAX calculated diffraction patterns, we used ProMAX's implementation of analysis described by Fergusen[15]. Chris Mack of FINLE Technologies has enhanced those calculations to compute transmission when the line and space are not 1:1 duty. For analyzing TEMPESTpr diffraction orders, we calculated effective phase shift according to a similar analysis by Peng, which assumes 1:1 duty. Experience showed that changing the line:space ratio input to ProMAX's diffraction pattern analysis changed transmission much more than phase, so for T EMPESTpr simulated masks with unequal line/space, the Peng approach was used to extract approximate phase but not transmission.

As a side note, it is important to highlight that a ProMAX mask must have a space, not a line, at x=0 for its phase and transmission analysis utility to function properly. Overlooking this point risks introducing sign errors to extracted phase and transmission results. If such mask files are exported in grayscale format (a file with intensity and phase at a z-plane in the 2D simulation), then one may wish to shift the x-coordinate data in the grayscale file to center the line at x=0 for PROLITH analyses. This applies to the January 21, 2001 and earlier versions of ProMAX.

Topography Optimization

Each mask type was optimized at 100nm:200nm line:space, and then the same adjustments were applied across pitch with fixed line size. As an example of optimization, the dual -trench with undercut mask type is instructive. In the search for the best approach for optimizing phase and transmission, we tried simply plotting effective phase and transmission vs. dual trench and undercut. Figure 5 shows the effective phase and transmission errors for dual trench masks vs. dual trench depth, before any phase trench correction was applied. In addition, figure 5 plots a range of undercuts simulated at two dual trench depths, 240nm and 270nm. Figure 5(b) shows the effect of undercut more directly. This figure suggests that to minimize both phase and transmission errors, a large undercut is needed. For masks using undercut but no dual trench correction, it is common to use a 100nm undercut. With dual trench and small line sizes, however, a 100nm undercut combined with greater than 200nm dual trench creates a chrome on glass structure with an aspect ratio that may be subject to lifting when cleaned. Because phase and transmission are coupled it can quickly become difficult to optimize both concurrently. For that reason, a single score was computed to combine phase and transmission error for each mask as follows:

$$score = |phase\ error / phase_scale_factor| + |transmission\ error| / (trans_scale_factor) \qquad (3)$$

where phase_scale_factor and trans_scale_factor are scale factors obtained by inspecting plots of relative magnitudes of observed phase and transmission errors. SF_phase was set to 9 degrees and SF_trans was set to 0.14 .

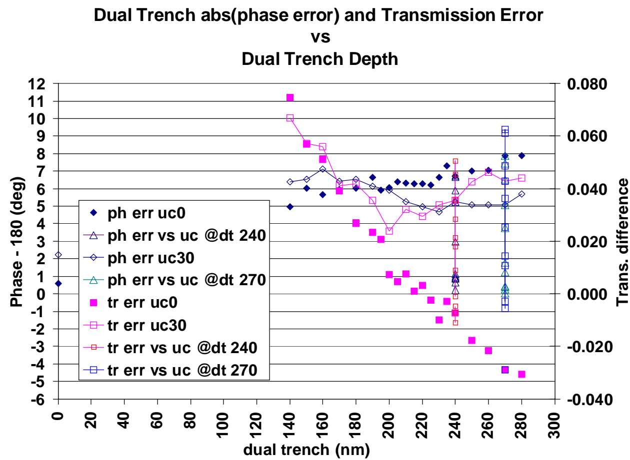

(a)

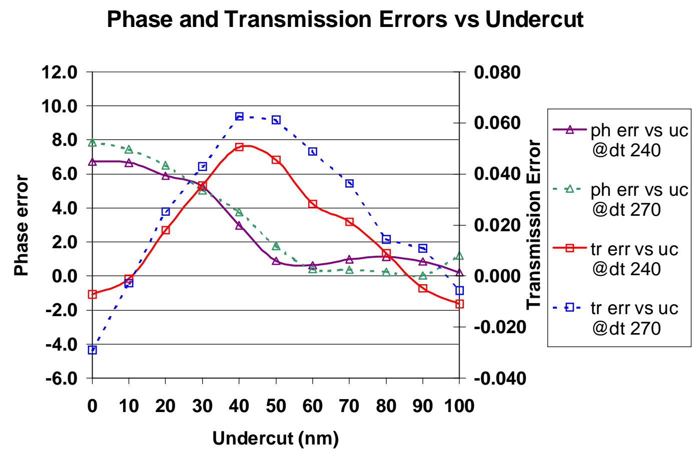

(b)

Figure 5: (a) Effective phase error (ph err) and transmission error (tr err) vs. dual trench (DT) depth with constant 180 degree mask design phase shift. (b) Phase and transmission errors vs. undercut (UC). In fig. 5(a), uc0 means 0nm undercut, and uc30 means 30nm undercut.

The scores for every dual trench / undercut / phase shift combination were ranked and the best were chosen for further phase optimization.

A more physically reasoned figure of merit than the score, though, is the ratio of central diffraction order power to the power in both first diffraction orders ("CPR," equation 2). Minimizing CPR will also minimize combined phase and transmission error. Figure 6 plots this power based figure of merit vs. dual trench depth and undercut, clearly identifying the most favorable conditions to explore. As outlined in Figure 5, the importance of adding undercut to dual trench is clear. Without undercut, no dual trench depth produces a power ratio approaching zero, meaning some phase or transmission error will remain. A similar conclusion on the importance of undercut was reached by Petersen et al [16] though in that work the deepest undercut was 40nm. They found best results using 240nm dual trench, 238nm shifter trench, and 0-15nm undercut. Also, they studied 1:1 duty 150nm line:space and their design criteria were lithographic log-slope and intensity imbalance at the wafer, rather than phase and transmission errors just below the 100:200nm line:space mask in our work. They did consider phase and transmission related corrections concurrently. In other similar dual trench (no undercut) work,

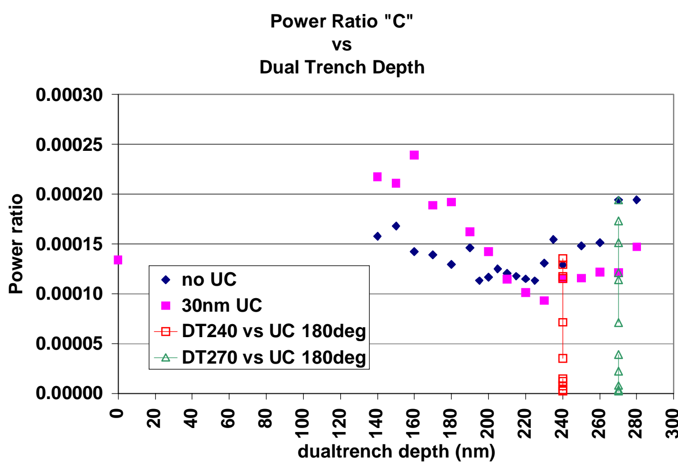

(a)

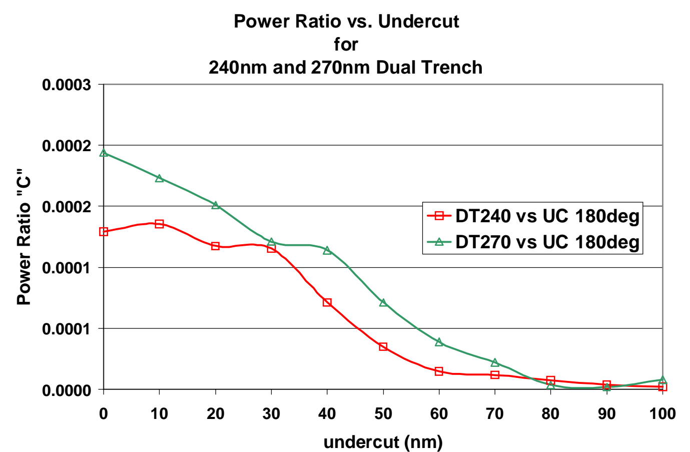

(b)

Figure 6: Power ratio “CPR” (from eq. 2) vs. undercut (UC) for two dual trench (DT) depths

Gordon et al[17] optimized dual trench at 270nm deep after first optimizing phase depth to 231nm. In comparison, the diffraction power based simulations in highlight the need to consider phase and transmission concurrently.

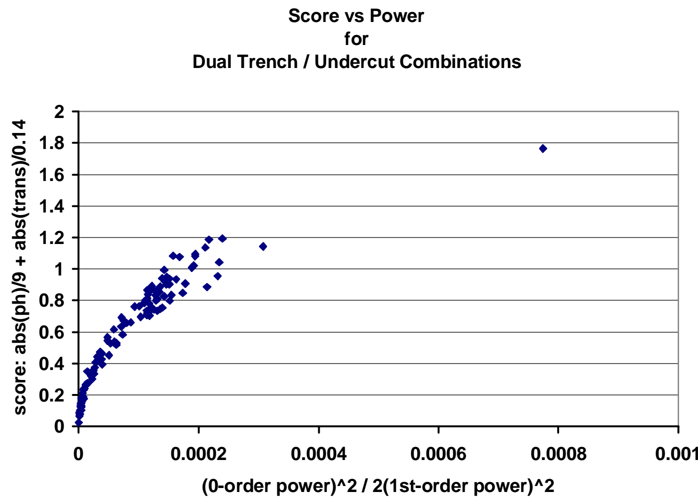

Figure 7: Score vs. Power Diffraction power in the central order vs. first orders (CPR, eq. 2) can be used as a single figure of merit to minimize phase (ph) and transmission (trans) errors.

Figure 7 was plotted to validate the diffraction power approach, and indeed, both phase and transmission errors are small when there is minimum power in the central order.
The best five candidates for dual trench / undercut were chosen using all three approaches discussed (plotting directly, computing a score, and computing a diffraction order power ratio), as well as by considering response slopes and desirability of shallow rather than deep undercuts. Then the phase shifting trench depth was varied for each of the five masks to minimize remaining phase error. The best depth was seen to be 251.6nm (173.8 degrees) for each of the five masks. The resulting mask candidates are listed in Table 1.

Condition	Sim ID	DT (nm)	UC (nm)	Power ratio CPR	Score	Effective phase	|Phase error|	Trans error
A	120	215	5	8.3E-08	0.02	179.9	0.1	0.002
B	102	225	20	8.7E-07	0.07	180.4	0.1	0.008
C	100	225	0	9.4E-07	0.08	180.5	0.5	0.004
D	93	215	10	1.0E-06	0.09	180.1	0.4	0.006
E	108	240	0	4.1E-06	0.18	180.9	0.9	-0.011

Table 1: The best five dual trench / undercut combinations based on power ratio and score at 300nm pitch only. The optimum shifter depth 251.6nm (173.8 degrees) for each of the five masks.

At this point the five candidates represented the 5 best dual trench / undercut / shifter depth combinations for a 100:200 line:space mask. The last step was to run the same combinations across a range of pitches from 200nm to 1100nm with fixed 100nm line. Figure 8 shows the results.

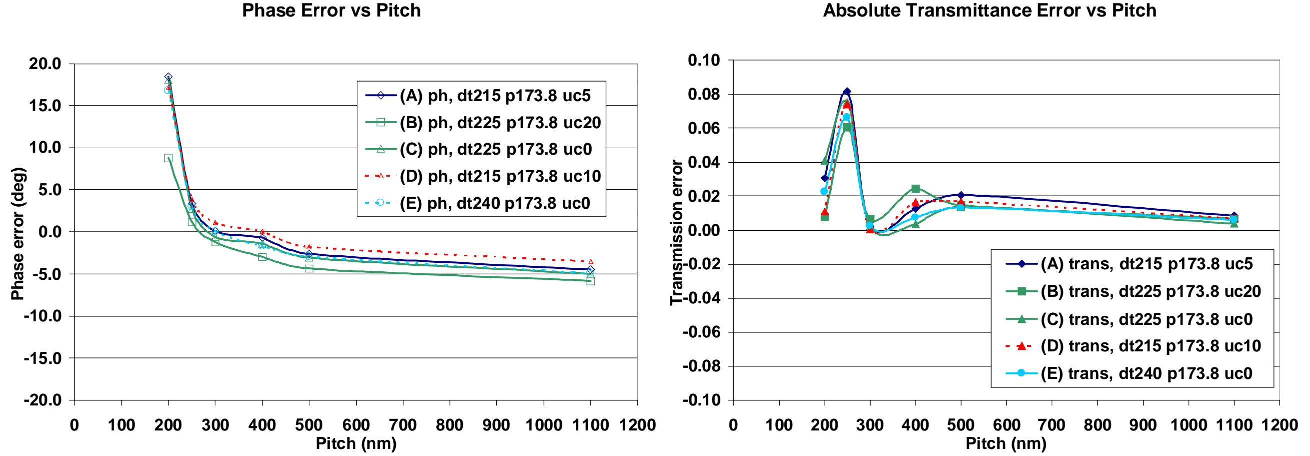

Figure 8: Across-pitch phase errors (ph) and absolute value of transmission errors (trans) for five candidate masks optimized for dual trench (dt), undercut (uc), and shifter design phase (p). Results for mask correction A were best at 300nm pitch.

To choose the best mask condition plotted in Figure 8, the across pitch ranges of phase error and transmission error were computed. Mask condition B ranks first according to both phase and transmission range across pitch. Another figure of merit, the across pitch power sum, was computed. The power sum was simply the sum of the power ratios at each pitch, or

$$power\ sum = \sum_{pitch\,1}^{pitch\,n} CPR_n \tag{4}$$

where CPR is the ratio of the power in the central diffraction order to the power in both first diffraction orders for a given mask, as defined in equation 3. Pitches ranged from 200nm to 1100nm, with fixed 100nm lines.

Correction	Across Pitch Performance		
	Phase Range (deg)	Trans Range	Power Sum
E	21.7	0.063	0.00049
B	14.6	0.054	0.00051
A	22.9	0.080	0.00061
C	23.0	0.073	0.00067
D	20.7	0.074	0.00069

Table 2: Across pitch performance of five dual trench / undercut combinations.

When corrections were ranked by power sum, (Table 2) mask E outperformed mask B, and both masks beat mask A (better at 300nm pitch). Correction B showed best phase and transmission error range but correction E performs best when the diffraction power ratio CPR is added across pitch. At this point, one should choose between the corrections by inspecting each point for each mask, but computing error ranges and power sums across pitch are both useful techniques to rank mask phase and transmission.

EMF Simulation Results for Each Mask Type

The techniques to optimize masks with dual trench, undercut, and shifter depth adjustments were applied to the other mask types where appropriate. Each mask type was optimized at 300nm pitch and then simulated across pitch, with the performance of selected mask types plotted in Figure 9 and graph legends explained in Table 3.

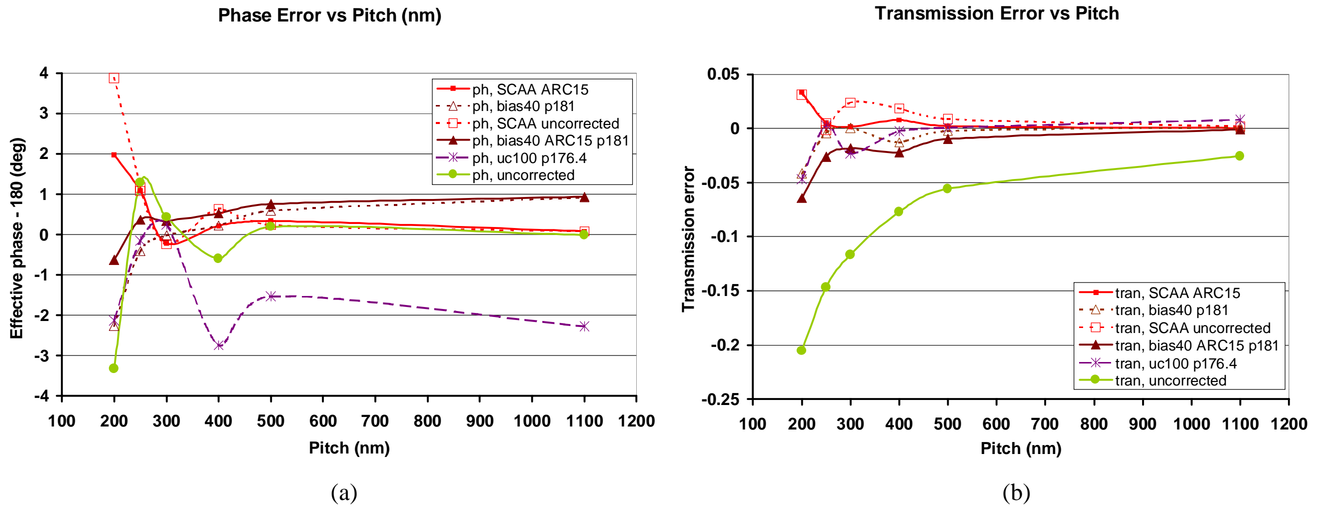

(a) (b)

Figure 9: Across pitch phase errors and transmission errors for selected mask types after optimization at 300nm pitch. Mask types were ranked according to power sum across pitch (equation 4). The best performing type was the SCAA mask with 15nm ARC, closely followed by the asymmetrically biased mask. The performance of an uncorrected mask is plotted for comparison.

Figure 9 legend	Mask type	Mask phase (deg)	Asymmetric Bias (nm)	Undercut (nm)	ARC (nm)
tran, SCAA ARC 15	SCAA	180			15
tran, bias40 p181	asymmetric bias	181	40		
tran, SCAA uncorrected	SCAA	180			
tran, bias40 ARC15 p181	asymmetric bias	181	40		15
tran, uc100 p176.4	undercut	176.4		100	
tran, uncorrected	no correction	180			

Table 3: Explanation of Figure 9 legend for phase error (ph) and transmission errors (tran). Mask types ordered according to sum power ratio across pitch.

Figure 9 shows that the SCAA and asymmetrically biased (where bias refers to the growth in each side of the shifting space) mask types perform well across pitch when both phase and transmission errors are examined. These two best masks were also simulated with an ARC to anticipate different results that might arise with an absorber more closely resembling that on commercial reticles. All other simulations in this work used 100nm of chrome with n and k parameters 0.85 and 2.01, while the ARC mask simulations used a film stack of 85nm chrome and 15nm topside ARC composed of CrO_3[18] with n and k values 1.72 and 0.39. This stack was simulated using PROLITH to have a reflectivity at $\lambda = 248$nm of 11.6%. With chrome ARC, the SCAA mask improved slightly, mostly in phase error at small pitch, while the asymmetrically biased mask was not as good as without ARC.

It is clear from Figure 9 that some mask structures, for example the undercut mask, would have better average errors if phase errors were biased up, that is if the shifter trench were made deeper. In the undercut case, optimizing for 300nm pitch did not result in the best average phase shift error attainable across pitch. The shift could be biased up in practice, with the understanding that both phase and transmission characteristics would change slightly because phase and transmission are coupled.

To rank each optimized mask type, the power sum was again computed for each type. Table 4 lists the ranking according to power sum, as well as optimized conditions for each mask type.

Mask type	Ranking	Mask phase (deg)	Shifter depth (nm)	Assym. Bias (nm)	Undercut (nm)	Dual trench depth (nm)	ARC (nm)	Across Pitch Range		Power Sum
								Phase (deg)	Trans.	
SCAA (ARC)	1	180	243				15	2.2	0.033	0.00002
Asymmetric bias	2	181	244.2	40				3.2	0.043	0.00004
SCAA (unadjusted)	3	180	243					4.1	0.033	0.00006
Asymmetric bias (ARC)	4	181	244.2	40			15	1.6	0.063	0.00007
Additive (unadjusted)	5	180	243					3.9	0.122	0.00014
Additive	6	182	245.7					5.4	0.098	0.00017
Undercut	7	176.4	238		100			3.0	0.055	0.00017
Dual-trench + Undercut	8	173.8	234.6		20	225		14.6	0.054	0.00051
Phase only	9	179.7	242.5					4.8	0.177	0.00076
No correction	10	180	243					4.6	0.180	0.00089
Dual trench	11	172.5	232.8			270		20.3	0.043	0.00123

Table 4: Optimized conditions for each mask type, with mask types ranked according to power sum (ratio of central diffraction order power to power in first orders, summed for each pitch).

Table 5 (below) displays the phase and transmission errors at each pitch, with mask types ranked the same as in Table 4. In addition, each error is assigned a "good, OK, or poor" rating. Industry guidelines consider a 2 degree phase error a reasonable spec limit. We assigned a “poor” to any phase error greater than 1.5 degrees. Table 5 shows that a dual trench correction performs well across pitch for transmission errors, but poorly for phase errors. Consequently, the power sum ranks it last, below even an uncorrected (or geometric) mask. The validity of this conclusion may change if an application does not require as wide of across pitch performance. The uncorrected mask suffered mostly from transmission errors. When only a phase correction was applied, meaning only the shifter depth was adjusted, the power sum improved slightly (see Table 4). Dual trench combined with undercut performed better than dual trench alone, but worse than undercut alone. Note that in undercut alone, we allowed a 100nm undercut, whereas the same undercut combined with a 225nm undercut would risk becoming too fragile to withstand mask cleaning processes. Allowing undercuts with dual trench greater than 80nm may improve performance. Still, as will be seen later, the dual trench technique also reduces the average aerial image intensity more than other approaches. The undercut alone mask is commonly built in mask shops. As mentioned earlier, it might be further optimized by fixing corrections at pitches other than the 300nm pitch chosen for this work. The next type, an additive shifter mask, performed closely to the undercut mask. It only required a shifter depth adjustment (to design shift at 182 degrees). An unadjusted additive mask actually performed better across pitch than the mask adjusted for 300nm pitch. Though this mask has promising simulations, however, it is not considered practical to build commercially.

Finally, the asymmetric biased mask and the SCAA mask (sidewall chrome alternating aperture) both performed better than other candidates. As mentioned earlier, these two masks were also simulated with chrome/ARC absorbers. The SCAA mask improved slightly with ARC whereas the asymmetric bias mask degraded slightly. Both types warrant further investigation. The asymmetric bias mask is simple to design and build, while SCAA masks require non-standard chrome deposition to shifter sidewalls. But an important point is that all masks in Table 5 except SCAA and an uncorrected mask required EMF simulations to optimize. Their results are a function of EMF simulator operation, input parameters such as chrome stack n and k parameters, and variation of physical mask parameters. SCAA performed at or near the best without any shifter, dual trench, undercut, or bias adjustments, and can therefore be expected to be less sensitive to fabrication and printing variations than other mask types. Quantifying the sensitivity of each mask type to fabrication tolerances thus warrants further study.

Correction Type	Pitch 200nm Ph	Pitch 200nm Tr	Pitch 250nm Ph	Pitch 250nm Tr	Pitch 300nm Ph	Pitch 300nm Tr	Pitch 400nm Ph	Pitch 400nm Tr	Pitch 500nm Ph	Pitch 500nm Tr	Pitch 1100nm Ph	Pitch 1100nm Tr
SCAA (ARC)	1.97	0.033	1.09	0.005	-0.21	0.002	0.22	0.008	0.34	0.002	0.08	0.000
Asymmetric bias	-2.26	-0.041	-0.41	-0.004	-0.02	0.000	0.22	-0.013	0.59	-0.002	0.92	0.001
SCAA (unadjusted)	3.88	0.031	1.17	0.005	-0.24	0.024	0.64	0.018	0.24	0.009	0.08	0.002
Asymmetric bias (ARC)	-0.62	-0.064	0.37	-0.026	0.34	-0.018	0.53	-0.022	0.76	-0.010	0.94	-0.001
Additive (unadjusted)	-3.83	0.120	-1.65	0.031	-1.41	0.001	-0.19	-0.002	-0.34	0.004	0.07	0.001
Additive	-3.55	0.099	-0.18	0.029	0.16	0.001	1.68	0.002	1.4	0.006	1.86	0.005
Undercut	-2.13	-0.047	-0.15	0.003	0.25	-0.023	-2.74	-0.003	-1.53	0.001	-2.27	0.008
Dual-trench + Undercut	-8.76	-0.008	-1.19	-0.060	1.21	-0.007	2.98	-0.024	4.35	-0.015	5.83	-0.007
Phase only	-4.09	-0.195	0.68	-0.136	-0.25	-0.108	-1.24	-0.068	-0.43	-0.046	-0.52	-0.017
No correction	-3.32	-0.205	1.29	-0.147	0.43	-0.117	-0.59	-0.077	0.19	-0.056	-0.01	-0.025
Dual trench	12.37	0.037	0.25	-0.007	-2.17	0.025	-5.22	0.000	-5.55	0.005	-7.89	0.000

KEY	|phase error|	|transmission error|
Good	0-.5	0-.025
OK	0.5-1.5	.025-.05
Poor	>1.5	>.05

Table 5: Phase and transmission errors for each optimized mask at each pitch.

3. IMAGING COMPARISON OF OPTIMIZED MASKS

Mask topographies were optimized and studied using EMF simulation with useful results. To see the relative lithographic impact of the phase and transmission errors just discussed in Table 5, we ran PROLITH simulations of the image placement errors that would arise from a range of mask phase and transmission errors. Then we selected two masks for further printability study. These two top ranking topographies from Table 5 were the SCAA mask with 15nm ARC and the asymmetric bias mask with 40nm bias on each side of shifter space. We input ProMAX EMF results to PROLITH in the form of a grayscale mask, which is a file containing intensity and phase at a plane just below the mask. The key analyses performed were NILS and MEEF.

Impact of Phase and Transmission Errors

We explored the relative importance of phase and transmission errors on lithographic performance by programming such errors into a scalar PROLITH mask and observing image placement error as the response to a focus-exposure simulation. The programmed errors and image placement results are shown in Table 6. Image placement results confirm that phase shift error must be controlled to limit image placement error, even with balanced transmission between shifted and unshifted spaces. If we compare the ranges of phase error partitioned in Table 5 to the phase errors in Table 6, we see that a 1.5 degree limit on phase error is reasonable. A 2 degree phase error would cause an 8nm image placement shift if there were also a 0.06 transmission mismatch, according to Table 6.

Image Placement Error (nm) vs Effective Phase Shift and Transmission mismatch

Effective Phase Shift (deg)	Shifted space transmission 0.94 min	0.94 max	0.97 min	0.97 max	1.00 min	1.00 max	Shifted space transmission 0.94 range	0.97 range	1.00 range
176	-1.6	7.7	-2.5	14.1	-3.1	12.0	9.3	16.6	15.1
178	0.0	8.2	-1.8	7.0	-1.1	5.7	8.2	8.8	6.8
180	1.3	1.3	1.0	1.0	0.0	-0.1	0.0	0.0	-0.1

Table 6: Image placement error vs. programmed mask errors in effective phase shift and transmission (ratio of unshifted to shifted space transmission).

NILS Comparison

SCAA with 15nm ARC and asymmetric bias were next compared for aerial image quality. The NILS through focus was computed at 300nm pitch and found to be identical for each mask. Of the two masks, SCAA showed less sensitivity of image CD to focus. Figure 10 plots these results.

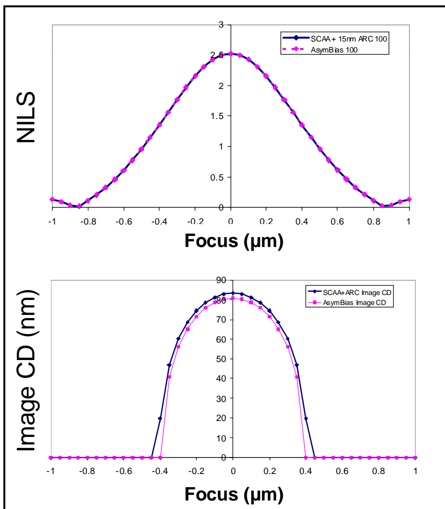

Figure 10: NILS and image CD through focus for asymmetric bias and SCAA masks..

MEEF Comparison

The top two ranked masks from Table 5 (SCAA and asymmetric bias) were simulated with line sizes 90nm, 100nm, and 110nm, and with spaces required to maintain 300nm pitch. Necessary EMF simulations were run and grayscale masks were created for input to PROLITH*. Focus-exposure matrices were created, while monitoring CD, sidewall angle, resist loss, and image placement. The simulation conditions for PROLITH 7.0 were illumination of 0.63 NA, 248nm, 0.30 sigma, and resist choice 304nm of UV113 on an ARC of 20nm of CD11 & 62.5nm AR-5. Next, the focus-exposure results were loaded into ProDATA** to analyze the process window using line CD and image placement as responses. An image placement spec was set at ± 5nm.

Figure 11 and Figure 12 show the process windows for the asymmetric bias mask and SCAA mask, respectively. Table 7summarizes the lithographic study numerically, and shows that both asymmetric bias and SCAA masks had similar MEEF of 0.9. The common process window was 0.3µm with 2% exposure latitude, which was driven by the fact that CD variation for the study was 10nm at the wafer, or 40nm at the reticle. A smaller CD range would be required for a production process. In addition, it was found that for single linewidths, 90nm and 100nm lines have 12 to 14% more depth of focus (DoF) on the SCAA mask than on the asymmetric biased mask. 110nm SCAA lines have 2.4% more DoF than asymmetric biased lines, limited by image placement on the SCAA mask, and more so on the asymmetric biased mask.

* Note to ProMAX and PROLITH users: ProMAX requires a mask to be arranged with a space centered at x=0 for the effective phase and transmission error to be extracted properly from the mask's diffraction pattern. When simulating line sizes in PROLITH, however, it is more practical to center the line in the center of the simulation window. For that reason we shifted the ProMAX x-coordinates in the grayscale data file so that the line was centered at x=0 before input to PROLITH.

** ProDATA is software from FINLE Technologies for analyzing lithographic data.

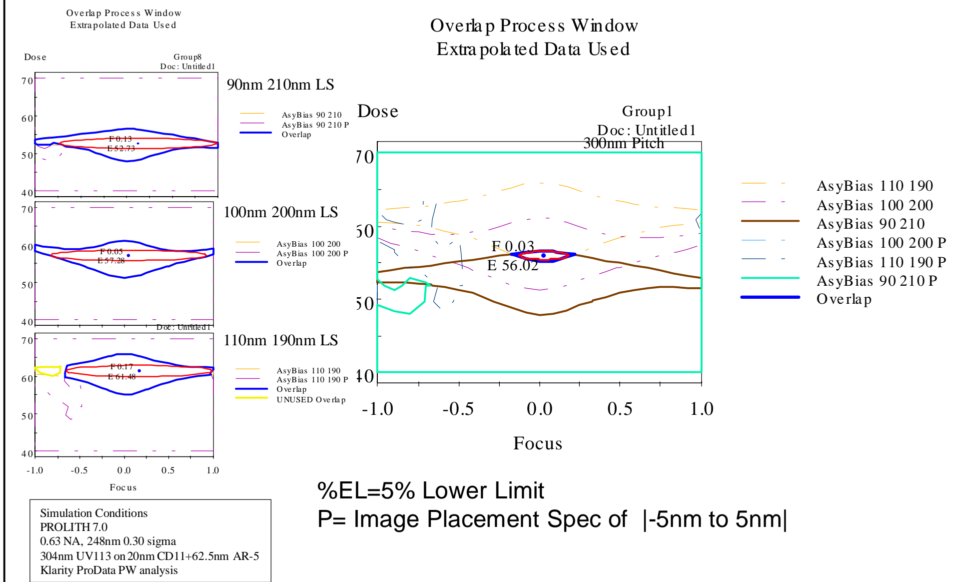

Figure 11: Asymmetric bias process window

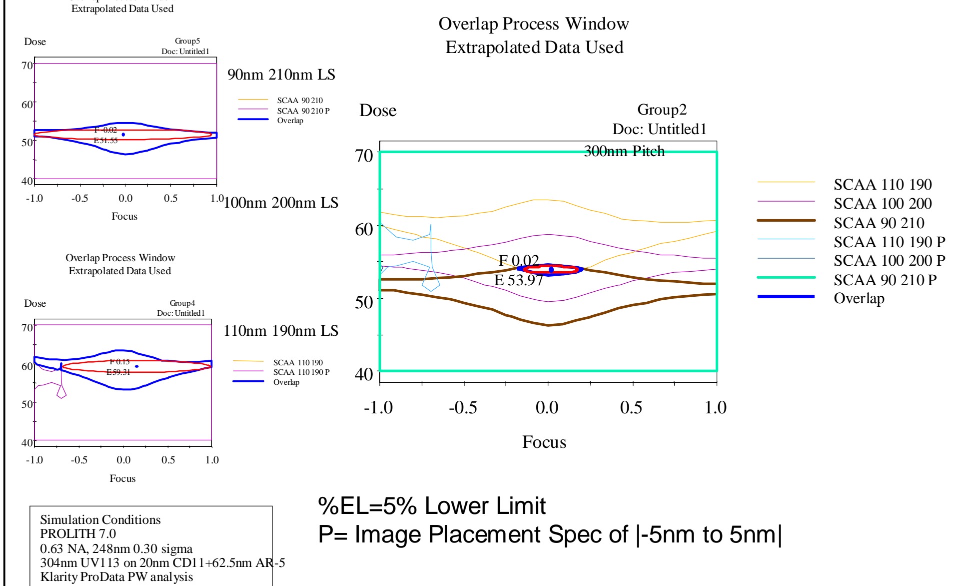

Figure 12: SCAA process window

MEEF Comparison Summary

- For the two best altPSM mask types, SCAA with 15nm Top ARC and 40nm Asymmetric Bias:
  - Similar MEEF of 0.9
  - Common process window of 0.3µm with 2% Exposure Latitude (%EL) for ±40nm mask CD variation.
  - Production process requires less than ±40nm mask CD variation.
- For SCAA performance within a single line:
  - 90nm and 100nm lines have 12 to 14% more DoF than AsymBias
  - 110nm lines have 2.4% more DoF than AsymBias
- 110nm line performance is limited by image placement for both masks, but AsymBias is the worst.

Type	Line Size 300nm Pitch	$E_{S=100nm}$	CD @ $E_{S=100nm}$	MEEF	$E_{PWCenter}$	DoF	w/X% EL	Phase Error	Tran Error
SCAA+15nm ARC	90.0		92.0		51.6	1.95	5	+0.25	-0.005
SCAA+15nm ARC	100.0	54.2	98.0	0.88	55.0	2	5	-0.21	0.002
SCAA+15nm ARC	110.0		109.0		59.3	1.67	5	-0.64	0.012
SCAA+15nm ARC	Common				55.0	0.3	2		
AsymBias	90.0		91.0		52.7	1.73	5	+0.21	-0.013
AsymBias	100.0	56.5	97.0	0.90	57.3	1.75	5	-0.02	0.000
AsymBias	110.0		109.0		61.5	1.63	5	+0.52	-0.005
AsymBias	Common				56.0	0.3	2		

Table 7: MEEF comparison results.

Both SCAA and asymmetric bias masks performed similarly with 0.9 MEEF. The common process window was 0.3µm with 2% exposure latitude. That is driven by the fact that CD variation for the study was 10nm at the wafer, or 40nm at the reticle. A smaller CD range would be required for a production process.

4. CONCLUSION

In this paper we have explored several approaches to correcting the phase and transmission differences that arise with a real mask compared to what is expected from simple scalar calculations. We pointed out the importance of optimizing the choice of simulator grid and described how we extracted effective phase and transmission errors directly from EMF simulated diffraction patterns.

We used a combination dual trench and undercut mask to show our approach, which was to optimize at 300nm pitch, and then apply the same corrections across pitch with fixed 100nm line size to show across pitch performance of various masks. A useful technique was found to be minimizing the ratio of central order diffraction power relative to power in the first orders, as a way to minimize phase and transmission errors concurrently. The final EMF results by mask type were ranked according to the sum of this power ratio across pitch, and we chose the two top mask types to examine with lithographic simulation. The two top ranking topographies were a SCAA mask using chrome ARC and an asymmetric bias mask. The SCAA mask had no trench depth or space width adjustments from scalar calculated values, while the asymmetric bias mask was made 40nm larger on each side of the shifter space, and had a designed phase trench of 181degrees for an effective shift of ~180 degrees. Neither mask used undercut. Other lithographers may rank the masks in this study differently according to their own criteria, but the techniques shown would remain useful.

PROLITH simulation showed that NILS through focus at 300nm pitch was identical for the SCAA and asymmetric biased masks, whereas image CD was less sensitive to focus on the SCAA mask compared to the asymmetric bias mask. These two masks also has similar MEEF of 0.9.

In sum, SCAA ranked best with no shifter depth or space width adjustments, while all other masks required EMF simulations and optimization. This advantage is contrasted by risk of increased manufacturing cost due to writing critical patterns late in the mask fabrication sequence. The closest contender, the asymmetric bias mask, requires no new mask shop processing such as SCAA's sidewall chrome deposition. SCAA's apparent advantages compel us to further investigate sensitivities to expected fabrication variations and to gain experience with wafer prints.

5. ACKNOWLEDGEMENTS

Chris Mack, FINLE Technologies, a division of KLA-Tencor, for ProMAX development and consulting
Tom Pistor, Panoramic Technologies for TEMPESTpr consulting.

6. REFERENCES

[1] M. D. Levenson, J. S. Petersen, D. J. Gerold and C. A. Mack, "Phase Phirst! An Improved Strong -PSM Paradigm", SPIE BACUS 2000, Monterey CA, paper 4186-42
[2] Peng, Song, “Through-Focus Image Balancing of Alternating Phase Shifting Masks”, SPIE Vol. 3873, p. 328-336 (1999)
[3] M.D. Levenson, N.S. Viswanathan, and R.A Simpson, "Improving Resolution in Photolitho graphy with a Phase-Shifting Mask," IEEE Trans. Electron Devices, Vol. 29, p.1812, (1982)
[4] M. Shibuya, "Projection Master for Transmitted Illumination" Japanese Patent Gazette # Showa 62-50811, application dated 9/30/80, issued 10/27/87.
[5] R. Ferguson, A. Wong, T. Brunner, and L. Liebmann, "Pattern-dependent correction of mask topography effects for alternating phase-shifting masks," SPIE, Vol. 2440, 349-360 (1995)
[6] T. Terasawa, N. Hasegawa, A. Imai, S. Okazaki, "Analysis of nonplanar topography effects of phase shift masks on imaging characteristic," Jpn. J. Appl. Phys, Vol. 34 pp. 6578-6583 (1995).
[7] H. Kanai, K. Kawano, S. Tanaka, E. Shiobara, M. Aoki, I. Yoneda, S. Ito, "Sub-quarter micron lithography with the dual-trench type alternating PSM," SPIE vol. 2793, p. 165 (1996)
[8] R. L. Gordon, C. A. Mack, and J. S. Petersen, "Design and analysis of manufacturable alternating phase -shifting masks", SPIE Vol. 3546, p. 606-616 (1998)
[9] J. S. Petersen, R. J. Socha, A. Naderi, C. Baker, S. Rizvi, D. VanDenBroeke, N. Kachwala, F. Chen, K. E. Wampler, R. Caldwell, S. Takeuchi, Y. Yamada, T. Senoh, M. McCallum, "Designing Dual-Trench Alternating Phase-Shift Masks for 140nm and Smaller Features Using 248nm KrF and 193nm ArF Lithography", SPIE Vol. 3412, p. 503-520 (1998)
[10] M.D. Levenson, "Phase shifting Mask Strategies: Isolated Dark Lines," Microlithography World 1, p. 6-12 (March/April 1992)
[11] Ibid. 2
[12] Private communication, Tom Pistor, Panoramic Technology, March 2001
[13] Bruce W. Smith, Lithography Research Group website at Rochester Institute of Technology, http://www.rit.edu/~lvz6961/, "Optical thin films for UV/VUV"
[14] Ibid. 2
[15] Ibid. 5
[16] Ibid. 9
[17] Ibid. 8
[18] Ibid. 13